How Does Surface Modification Aid in the Dispersion of Carbon Nanofibers?

Jian Zhao,[†] Dale W. Schaefer,*[,†,§] Donglu Shi,*[,†] Jie Lian,[||] Janis Brown,[‡] Gregory Beaucage,[†] Lumin Wang,[||] and Rodney C. Ewing[||]

Department of Chemical and Materials Engineering, University of Cincinnati, Cincinnati, Ohio 45221-0012, Air Force Research Laboratory, Materials and Manufacturing Directorate, MLBCO, WPAFB, Ohio 45433-7750, Manuel Lujan Jr. Neutron Scattering Center, Los Alamos National Laboratory, Los Alamos, New Mexico 87545, and Departments of Geological Science and Materials Science & Engineering, University of Michigan, Ann Arbor, Michigan 48109

Received: September 11, 2005; In Final Form: October 24, 2005

Small-angle light scattering is used to assess the dispersion behavior of vapor-grown carbon nanofibers suspended in water. These data provide the first insights into the mechanism by which surface treatment promotes dispersion. Both acid-treated and untreated nanofibers exhibit hierarchical morphology consisting of small-scale aggregates (small bundles) that agglomerate to form fractal clusters that eventually precipitate. Although the morphology of the aggregates and agglomerates is nearly independent of surface treatment, their time evolution is quite different. The time evolution of the small-scale bundles is studied by extracting the size distribution from the angle-dependence of the scattered intensity, using the maximum entropy method in conjunction with a simplified tube form factor. The bundles consist of multiple tubes possibly aggregated side-by-side. Acid oxidation has little effect on this bundle morphology. Rather acid treatment inhibits agglomeration of the bundles. The time evolution of agglomeration is followed by fitting the scattering data to a generalized fractal model. Agglomerates appear immediately after cessation of sonication for untreated fibers but only after hours for treated fibers. Eventually, however, both systems precipitate.

Introduction

Although hundreds of papers have been published describing enhanced dispersion of carbon nanotubes by surface modification, the nature of the dispersed entities remains unknown. Dispersion is typically assessed by drying the solutions and observing the residual carbon by electron imaging, providing indirect evidence regarding the fluid state. Here we use light scattering to infer the morphology of the dispersed vapor-grown carbon nanofibers (VGCNF). The time evolution of the scattering data shows that surface treatment inhibits large-scale carbon agglomeration, but has minimal effect on the short-scale bundling of tubes that has dominated interpretation of imaging data.

In the untreated state, both single-walled nanotubes and VGCNFs can be dispersed with sonication since the external mechanical energy overcomes attractive van der Waals forces. However, nanotubes do not remain suspended in quiescent (unsonicated) suspension at any significant concentration.[1,2] Intense ultrasound can aid dispersion, but sonication also induces defects in nanotubes.[3] Appropriate chemical oxidation of nanotube surfaces, with the aid of prolonged sonication in a mixture of concentrated sulfuric acid and nitric acid, creates surface acid sites, which are mainly carboxylic in nature, on both the internal and external surfaces of the nanotubes.[4−6 7] Such modification renders the tubes hydrophilic and thus aids dispersion.

A 3:1 concentrated H_2SO_4:HNO_3 mixture is commonly used for modification because it can intercalate and exfoliate graphite.[8] By controlling the reaction conditions during acid treatment, nanotubes can be either shortened (100−300 nm) or kept at full length (>2 μm).[4,5,9] The tube tips and defects on the sidewalls are vulnerable areas to oxidative attack.[10−12]

After acid treatment, nanofibers form relatively stable colloidal solutions in water. Dispersions have been characterized by atomic force microscopy (AFM), UV/visible−NIR spectra, etc.[11,13] The evolution of the dispersed state under quiescent conditions following sonication, however, remains unknown. We recently used scattering to determine the morphology of carbon nanotube suspensions.[14,15] In this paper, we use this tool to quantify the state dispersion of as-received and acid-treated carbon nanofibers as a function of time. To understand the state of aggregation of the nanofibers, the size distribution from the light scattering data is determined using the maximum entropy (ME) method.[16−18] We used the Irena code (http://www.uni.aps.anl.gov/~ilavsky/irena.html) developed by Ilavsky and Jemian to obtain the maximum-entropy solution.[19,20]

Experimental Section

Vapor-grown nanofibers were provided by Applied Sciences, Inc., Cedarville, OH. Pyrograf-III PR19LHT nanofibers are vapor grown and subsequently heated to temperatures up to 1600 °C. The Pyrograf-III VGCNF normally contain a few concentric cylinders but may also be nested truncated cones. Typically the cores are open.

The nanofibers were treated to attach carboxylic acid groups to their surfaces. The acid-treated nanofibers were prepared as follows: A 100-mg portion of nanofibers was added to 400 mL of a mixture of 98% H_2SO_4/70% HNO_3 (3:1). The mixture

* To whom correspondence should be addressed. E-mail: dale.schaefer@uc.edu.
[†] University of Cincinnati.
[‡] Air Force Research Laboratory.
[§] Los Alamos National Laboratory.
[||] University of Michigan.

10.1021/jp055129f CCC: $30.25
Published on Web 11/22/2005

was subject to ultrasonication for 4 h at 10 W. The resulting mixture was diluted with deionized water to 2000 mL and then filtered through a poly(tetrafluoroethylene) membrane disk filter (Gelman, 0.2-μm pore size) followed by washing several times with deionized water until no residual acid was present.

Transmission electron microscopy (TEM) samples were prepared by allowing a drop of nanofiber suspension to dry onto Cu grids with holy carbon film. The high-resolution TEM (HRTEM) experiments were performed using a JEOL JEM 2010F electron microscope with a field emission source. The accelerating voltage was 200 kV.

The dispersion efficiency was determined using a low-angle light-scattering photometer-a Micromeritics Saturn Digitizer (www.micromeritics.com). The data are reported in reciprocal space as intensity vs the magnitude of the scattering vector, q. Light scattering covers the regime 10^{-6} Å$^{-1} < q < 10^{-3}$ Å^{-1}, where $q = (4\pi \sin \theta)/\lambda$, θ being half the scattering angle and λ the wavelength of the radiation in the medium. This q range corresponds to length scales ($\sim q^{-1}$) from 100 μm at low q to 1000 Å (0.1 μm) at high q.

Results and Discussion

The raw Pyrograf-III PR19HT powder consists of loosely aggregated nanofibers. Some nanofibers are curved with open ends. A representative HRTEM image of the original Pyrograf-III PR19HT (Figure 1) shows the graphite structure with the interlayer spacing $d = 0.34$ nm. No iron catalyst particles are found by TEM. Defects on the walls of nanofibers are occasionally observed in pristine nanofibers.

Bright field and HRTEM images of the acid-treated nanofibers are shown in Figure 2. More defects and even serious damage are found after the acid treatment. Disruption of outer graphitic layers is also observed. The stripping of the altered outer graphite layers after strong oxidation can give rise to thinning of nanofibers. These observations are consistent with the literature.[11,21]

There is considerable experimental evidence for the presence of carboxylic acid bound to carbon nanotubes through acid treatment.[4,22] These carboxylic groups result in improved dispersion of carbon nanotubes in polar solvents. The carboxylated carbon nanofibers are stable in water for days. In the absence of sonication, however, tubes eventually aggregate and precipitate. We use light scattering to monitor this process.

Figure 3 shows the light scattering profiles as a function of time for acid-treated nanofibers in water at a concentration of 5.0×10^{-6} g/mL. The data were obtained in the batch mode with no circulation or sonication. Initially the scattered intensity at low q decreases up to 8 h. Below we argue that this decrease is due to settling with minimal agglomeration. After 8 h, however, the intensity increases substantially at low q, consistent with agglomeration. In dilute solution the intensity at $q \rightarrow 0$ is proportional to molecular weight, so the data in Figure 3 imply an increase of molecular weight by a factor of 10 between 8 and 44 h.

Except for the data near 8 h, two "knees" are observed indicating two length scales. The knee region is referred to as Guinier scattering. The curvature in the Guinier regime defines a length scale (Guinier radius or radius-of-gyration, R_g, in the case of independent scatterers). Each Guinier knee is followed by a quasi-power-law regime. The curves were fit using Beaucage's unified model to extract R_g, the power-law exponents, P, and the Guinier prefactors, G, and power-law prefactor, B, associated with each length scale.[23] These parameters are displayed in Table 1 for the two structural levels. The slope

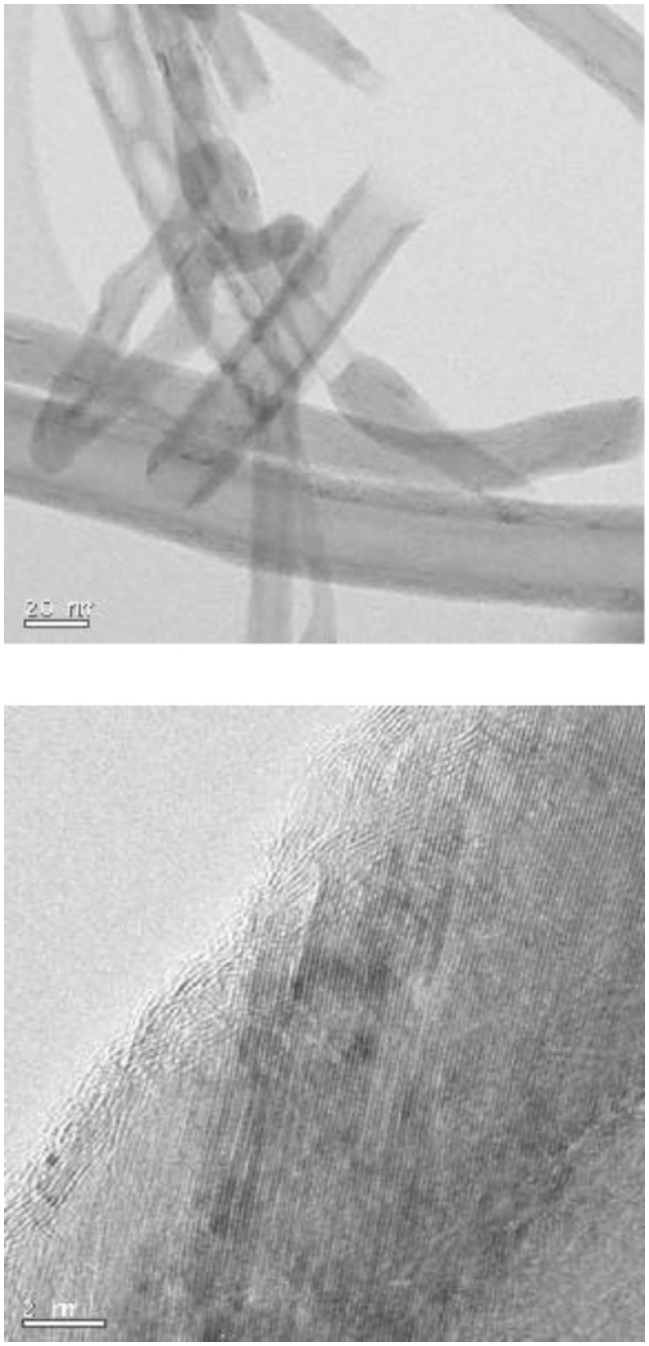

Figure 1. Bright-field (top) and high-resolution (bottom) TEM images of unmodified carbon nanofibers PR19LHT. Graphitic layers are visible at both magnifications. The low-resolution image shows a variety of tube shapes and morphologies including concentric cylinders and stacked cones. No metallic catalyst was observed. The bars are 20 and 2 nm.

near -2 ($P = 2$) on a log$-$log plot around $q = 0.002$ Å^{-1} could arise from a hollow tube since the wall of such an object is two-dimensional on scales larger than its wall thickness and shorter than the radius. Such a slope, however, can also arise from more complex aggregated structures.[14,15] The crossover length scale ($q^{-1} \cong 1$ μm) between the two power-law regimes corresponds to the largest radius of the tube aggregates. Minimal change in R_g and P is observed for $q > 10^{-4}$ Å^{-1}, indicating minimal change in morphology with time on length scales below ~ 1 μm.

The prefactor, G, derived from high-q structural level (level 1) decreases up to 8 h, indicating that the number and/or molecular weight of the small-scale entities is decreasing up to

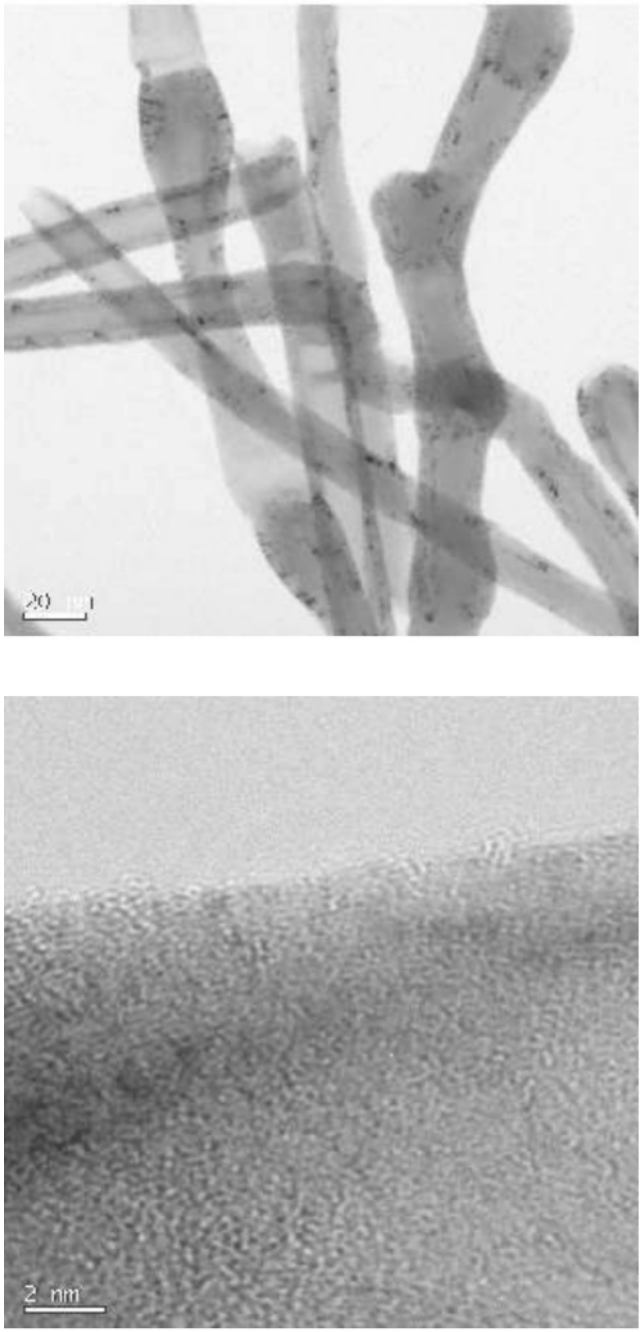

Figure 2. Bright-field (top) and high-resolution (bottom) TEM images of acid-treated carbon nanofibers: More defects on the walls are evident and breakage of graphite layers. The bars are 20 and 2 nm.

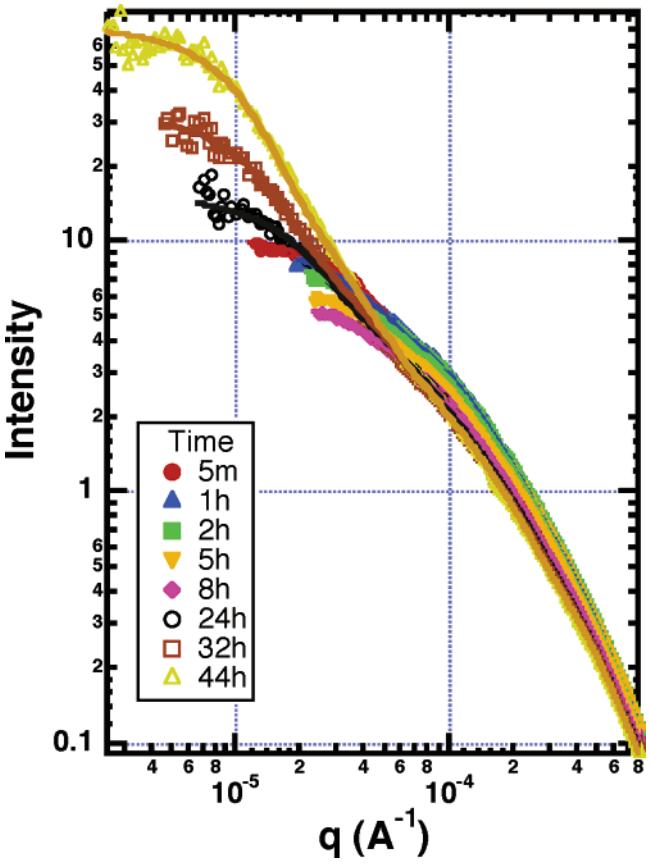

Figure 3. Dispersion of acid-treated nanofibers in water during two-day suspension. The suspensions were sonicated at 10 W for five minutes before data were taken using light scattering in batch mode. Minimal change is observed at large q indicating minimal change in morphology below 1 μm. The micrometer-sized entities originally present simply aggregate into larger structures in a hierarchical fashion. The lines are two-level unified fits. The unified parameters are collected in Table 1. Low-q data are absent in regions where the signal is not significantly above background.

TABLE 1: Guinier Radii and Exponents as a Function of Time for Acid-Treated Carbon Nanofibers

	time	5 min	1 hr	2 hr	5 hr	8 hr	24 hr	32 hr	44 hr
low q	R_g (μm)	4.8	4.6	4.5	4.3	3.5	8.4	11.9	14.4
	P	1.04	1.07	1.09	1.01	1.00	1.29	1.45	1.78
	G	9.5	8.7	8.5	7.2	4.6	14.0	30.5	69.1
	10^5 B	6.33	9.89	2.75	5.28	1.94	0.94	0.45	0.006
high q	R_g (μm)	0.80	0.83	0.78	0.75	0.86	0.79	0.77	0.87
	P	2.10	2.13	2.15	2.03	2.09	2.00	2.08	2.07
	G	0.87	1.15	0.72	0.42	1.30	0.97	1.04	1.61
	10^8 B	3.25	2.72	2.82	4.01	3.35	6.09	3.14	3.29

8 h. After 8 h, however, the data indicate that these small-scale structures cluster form large-scale objects, which we call agglomerates. All the carbon precipitates after several days. Chen et al. observed similar behavior in the region $2 \times 10^{-4} < q < 2 \times 10^{-3}$ for single-walled nanotube suspensions.[24]

We also monitored dispersion behavior of untreated carbon nanofibers although such a suspension is quite unstable in water even with aid of ultrasound. The data for the untreated sample (Figure 4) show similarities and differences when compared to the treated sample. Although less visible, two structural levels are present and the length scales are similar to the treated case in Figure 3. For the as-received sample, however, the large-scale agglomerates are observed immediately (5 min), whereas they form after 8 h in the treated case. Acid-treatment retards this agglomeration. The overall intensity also shows a nearly monotonic trend with time to lower values consistent with precipitation being the dominant process. The extracted R_g values are virtually unchanged during the precipitation process. The similarity of the length scales for the treated and untreated samples shows that acid treatment does not change the gross morphology of the nanofiber aggregates but only inhibits agglomeration of these smaller scale aggregates. Figure 5 compares the scattering profile for acid-treated and as-received carbon nanofibers at 5 min after sonication. The intensity at low q (prefactor, G) for the acid-treated sample is 1 order of magnitude smaller than that for the untreated one, indicating smaller entities in former suspension. Detailed analysis shows that the low-q Guinier radius is 4.8 μm for acid-treated nanofibers, compared to 21.3 μm for untreated nanofibers. These observations are consistent with improved dispersion due to the presence of oxygen-containing functional groups on the surface.

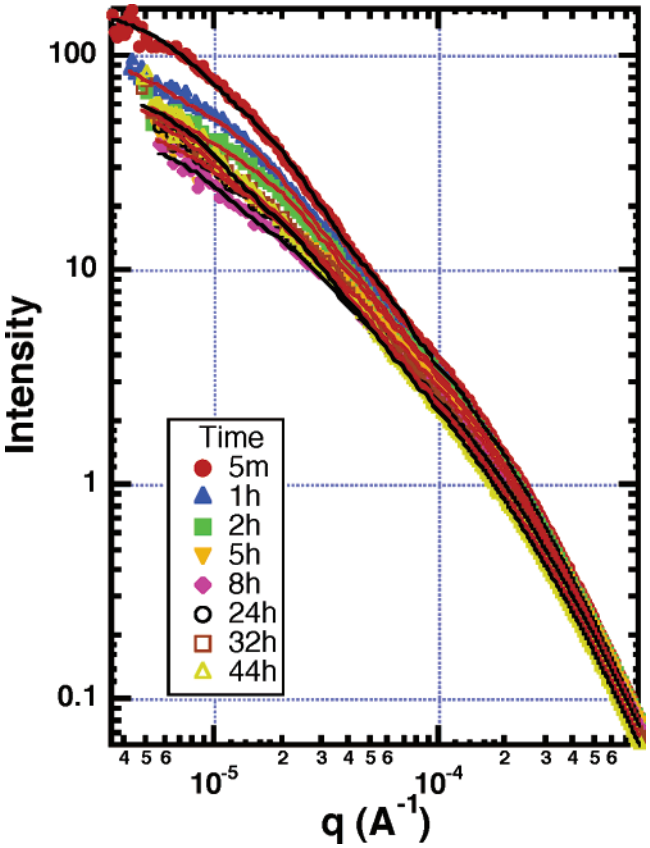

Figure 4. Evolution of the light-scattering profile of unmodified nanofibers for 2 days following dispersion by sonication. The suspensions were sonicated at 10 W for five minutes before the observations began. The measurements were taken in the batch mode, so the sample was undisturbed during the course of the experiment. Note that the intensity at small q is a factor of 10 larger than Figure 3, implying larger aggregated structures. The lines are two-level unified fits. The unified parameters are collected in Table 2.

TABLE 2: Guinier Radii and Exponents as a Function of Time for As-Received Carbon Nanofibers

	time	5 min	1 hr	2 hr	5 hr	8 hr	24 hr	32 hr	44 hr
low q	R_g (μm)	21.3	20.9	20.8	19.4	18.6	19.5	20.1	20.2
	P	1.48	1.44	1.43	1.22	1.23	1.32	1.35	1.40
	G	160.2	110.1	74.2	51.5	44.9	65.2	70.1	74.3
	10^6 B	0.59	4.23	4.14	29.72	23.24	10.67	8.30	4.43
high q	R_g (μm)	0.86	0.84	0.88	0.83	0.87	0.83	0.83	0.82
	P	2.01	2.07	2.15	2.14	2.08	2.00	1.98	2.10
	G	1.53	1.24	1.46	0.92	1.00	0.67	0.66	0.69
	10^8 B	4.53	2.93	1.67	1.77	2.56	3.90	4.75	1.89

In principle, the morphology of both the small and large-scale objects can be inferred from the power-law exponents, P, since P is the fractal dimension, D, of the objects giving rise to the scattering. $D = 1$ implies a linear object, and $D > 1$ indicates more branched or flexible structures.[14,15] For our data, however, the scattering entities are polydisperse and the power-law regions extend over a very limited q range, so this approach is unworkable. An alternative is to use the relationship, $M_w \approx R_z^D$, where M_w is the weight-average molecular weight, R_z is the weight-squared-average radius, and D is the fractal dimension of the object. Since $G \approx M_w$ and $R_z \approx R_g$, D can be extracted from the slope of a log−log plot of G vs R_g. Such a plot is shown in Figure 6 for the two structural levels for both the treated and untreated samples. Except for the low-q data for the treated sample, the data imply $D \geq 6$, which is unphysical. When the slope is greater than 3 we interpret the evolution of the scattering profile as due to precipitation of carbon, because,

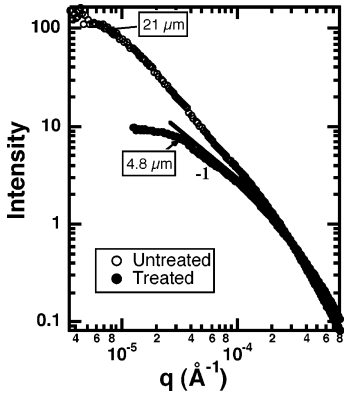

Figure 5. Comparison of the scattering profiles for untreated and acid-treated carbon nanofibers 5 min after sonication. A substantial population large-scale clusters is present only for the untreated sample.

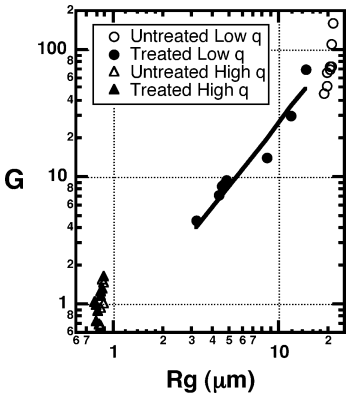

Figure 6. Relationship between the Guinier prefactors and the Guinier radius for two structural levels observed in Figures 4 and 5. The low-q result for the treated sample is consistent with agglomeration to form a fractal cluster with fractal dimension $D = 1.7$. In the other cases, the large change in G with minimal change in R_g is consistent with sedimentation.

to first approximation, G simply decreases at fixed R_g. For the untreated samples, therefore, both structural levels evolve by precipitation.

For the treated sample, the small-scale objects precipitate for the first 8 h and then begin to agglomerate. The latter conclusion is reached because $D = 1.7 \pm 0.15$ for the large-scale structure (Figure 6), consistent with a fractal morphology characteristic of agglomerates formed by kinetic growth. This number is also consistent with the value of P in Table 1 for the 44-h-treated sample. For the other times, the power-law region is insufficient to compare the measured P values and D from Figure 6. For the treated sample, precipitation dominates agglomeration up to 8 h and agglomeration dominates precipitation after 8 h.

To further understand the morphology evolution, the data were analyzed to estimate the bundle size distributions using the maximum-entropy method. To extract the size distribution a particle shape must be assumed. Electron microscopy shows that carbon nanofibers are tubelike with some fibers showing more rodlike character. The high-q feature of the data should arise from this one-dimensional morphology.

We investigated both rod and tube models as shown in Figures 7 and 8, which compare the two models for the 8-h acid-treated sample. Figure 7 shows the fits to the light-scattering data. Figure 8 shows the corresponding volume distributions assuming both rod and tube form factors. In the tube case, distributions calculated for different tube-wall thicknesses are shown. For the tube model the fits to the scattering profiles are virtually independent of wall thickness, although the volume

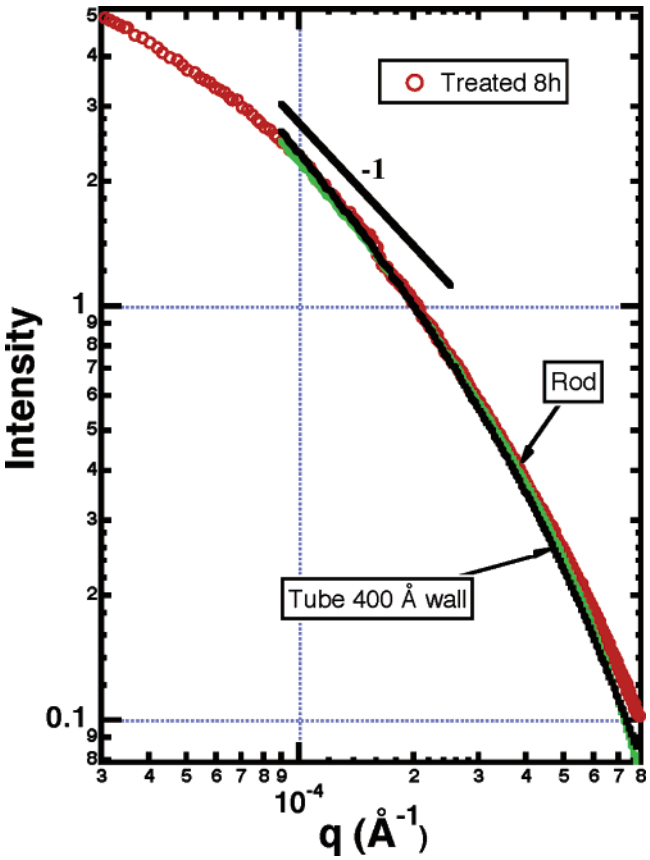

Figure 7. Maximum-entropy fits to the 8-h treated data assuming rods and tubes. The tube fit is virtually independent of the assumed tube wall thickness. Both rods and tube distributions fit equally well.

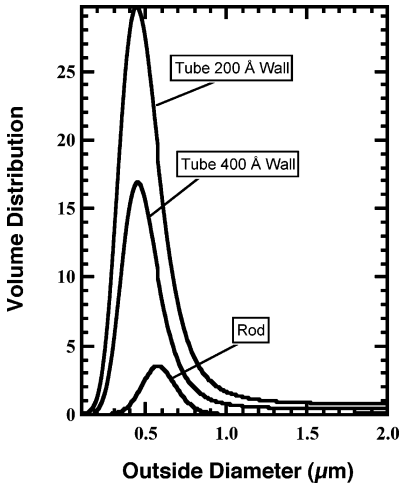

Figure 8. Volume distributions assuming rods and tubes for the 8-h acid-treated data. Both models show diameters somewhat larger than that observed by TEM, indicating some (side-by-side) aggregation.

distributions show a change in amplitude consistent with the increase of molecular weight with wall thickness, the solid rod being the limiting case. The position and shape of the distribution does not depend strongly on the assumed form factor.

Unfortunately virtually any form factor can be used to generate a size distribution using the maximum entropy method on such featureless data. Therefore, on the basis of the fits, it is impossible to distinguish between rods and tubes or for that matter more complex structures. Both models give similar results with a peak in the diameter distribution around 0.5 μm. In all cases, the diameter at the peak is considerably larger than the tube diameters seen in TEM. The scattering entities are not individual tubes but bundles thereof.

Interestingly, the size distributions (Figure 9) extracted from these high-q data show minimal change with time implying that the short-scale morphology is maintained during agglomeration and precipitation. Both the peak position and the tails to larger sizes indicate that dispersion is not complete, based on the tube diameters seen in TEM. The bias to larger sizes is likely due to side-by-side fiber aggregates that are never disrupted. Because light scattering is weighted by volume, it does not take much aggregation to produce such tails on the size distributions.

Comparison of parts a and b of Figure 9 shows that the large-diameter wing of the distribution is suppressed in the acid-treated sample. That is, acid treatment breaks up the larger aggregates. Since the contrast is not known, the volume distributions (ordinate in Figure 9) are on an arbitrary scale. Nevertheless, comparison of the distributions in Figure 9 is meaningful. On the basis of this comparison, the volume missing from the large-diameter wings of the treated distributions shows up at around 0.4 μm, which is still substantially larger than the largest individual fibers seen in TEM.

The simplified rod and tube models used here were developed by Justice and Schaefer.[25] These models approximate the exact rod and tube models in various power-law regimes and give the proper crossover length scales. Exact models, however, display oscillations in the power-law regimes, which are suppressed in the simplified models. This simplification is of minimal consequence when dealing with polydisperse distributions but it does accelerate the maximum entropy code.

Determination of the size distribution for the low-q data is more challenging. In fact, we are not able to extract reasonable size distributions from the low-q portion data using a fractal aggregate model. The process of dispersion and precipitation, however, can be inferred from time evolution of R_g and G extracted from the low-q unified fits. These parameters are found in Table 1.

Figures 10 and 11 show R_g and G derived from the low-q region as function of time for acid-treated and untreated nanofibers. For the untreated fibers, G decreases at nearly constant R_g, consistent with precipitation. After 10 h, both R_g and G stabilize. For the treated case, G and R_g increase with time consistent with agglomeration. It is interesting that, after 44 h, these parameters approach that of the untreated fibers. These observations are consistent with the fact that acid treatment slows agglomeration and precipitation, but ultimately the fate of the treated fibers is the same as that of the untreated.

Conclusion

We compare dispersion behavior of acid-treated and as-received carbon nanofibers suspended in water under quiescent conditions. Both samples show a hierarchical morphology consisting small-scale aggregates and large-scale agglomerates. The aggregates could be side-by-side bundles of individual nanofibers or more complex structures. In any case these objects agglomerate to form large-scale fractal clusters. Acid treatment shifts the small-scale size distributions to smaller bundle sizes. In the absence of surface treatment, these bundles agglomerate immediately after sonication. In the acid-treated case, by contrast, it takes many hours for the agglomerates to form. Thus acid treatment assists dispersion primarily by retarding large-scale agglomeration not by suppressing small-scale aggregation.

These observations are probably applicable to other forms of surface treatment. Although surface treatment does break up the small-scale aggregates to some extent, substantial aggrega-

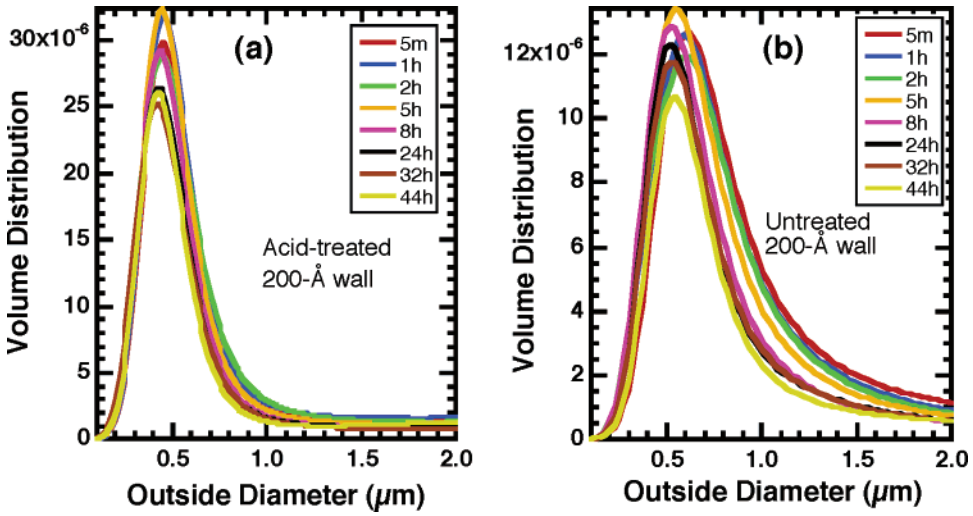

Figure 9. (a) High-*q* volume distributions as a function of time for acid-treated nanofibers. The curves are obtained by ME method from light-scattering data in the high-*q* region. The particle shape used is tube. The ordinate is arbitrary in that the contrast is not known. (b**)** High-*q* volume distributions for untreated nanofibers. The curves are obtained by ME method from light-scattering data in the high-*q* region. The particle shape used is tube. Although the ordinate is in arbitrary units, the distributions can be quantitatively compared to Figure 9.

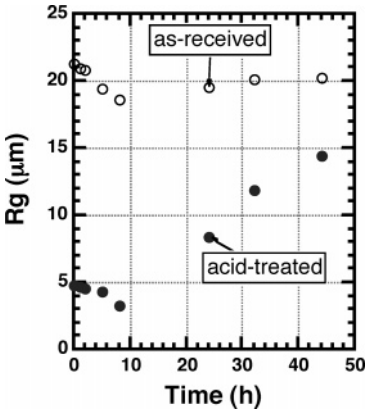

Figure 10. Apparent radius-of-gyration derived from the low-*q* region as a function of time for untreated and acid-treated nanofibers.

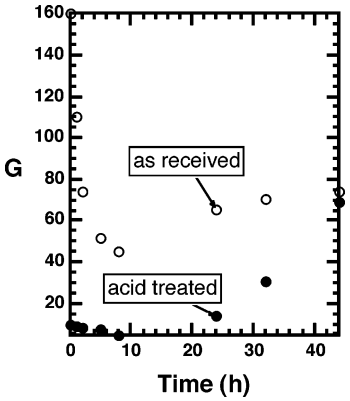

Figure 11. Guinier prefactor derived from the low-*q* region as a function of time for untreated and acid-treated nanofibers. At a given concentration *G* is proportional to the molecular weight.

tion exists even after treatment as evidenced by Figure 9. This behavior is probably due to the fact that modification is restricted to assessable areas of the tubes. Side-by-side aggregates, for example, may not be modified in the region of contact, which would account for the fact that modification has minimal impact on the size of the small-scale bundles. Modification does alter external surfaces of bundles, which leads to inhibition of agglomeration. Suppression of agglomeration is the primary mechanism by which surface treatment assists dispersion. Ultimately, however, the fate of both treated and untreated fibers is the same: agglomeration to form fractal clusters that eventually precipitate.

Acknowledgment. Work at the University of Cincinnati was supported by the University of Dayton Research Institute. The facilities of the Manuel Lujan Jr. Neutron Scattering Center are gratefully appreciated. This work was supported in part by the Office of Basic Energy Science, U.S. Department of Energy.

References and Notes

(1) Hobbie, E. K.; Wang, H.; Kim, H.; Han, C. C.; Grulke, E. A.; Obrzut, J. *Rev. Sci. Instrum.* **2002**, *74*, 1244.

(2) Jiang, L.; Gao, L.; Sun, J. *J. Colloid Interface Sci.* **2003**, *260*, 89.

(3) Lu, K. L.; Lago, R. M.; Chen, Y. K.; Green, M. L. H.; Harris, P. J. F.; Tsang, S. C. *Carbon* **1996**, *34*, 814.

(4) Liu, J.; Rinzler, A. G.; Dai, H. J.; Hafner, J. H.; Bradley, R. K.; Boul, P. J.; Lu, A.; Iverson, T.; Shelimov, K.; Huffman, C. B.; Rodriguez-Macias, F.; Shon, Y. S.; Lee, T. R.; Colbert, D. T.; Smalley, R. E. *Science* **1998**, *280*, 1253.

(5) Chen, J.; Hamon, M. A.; Hu, H.; Chen, Y. S.; Rao, A. M.; Eklund, P. C.; Haddon, R. C. *Science* **1998**, *282*, 95.

(6) Baughman, R. H.; Cui, C. X.; Zakhidov, A. A.; Iqbal, Z.; Barisci, J. N.; Spinks, G. M.; Wallace, G. G.; Mazzoldi, A.; De Rossi, D.; Rinzler, A. G.; Jaschinski, O.; Roth, S.; Kertesz, M. *Science* **1999**, *284*, 1340.

(7) Lin, Y.; Rao, A. M.; Sadanadan, B.; Sun, Y. P. *J. Phys. Chem. B* **2002**, *106*, 1294.

(8) Bower, C.; Kleinhammes, A.; Wu, Y.; Zhou, O. *Chem. Phys. Lett.* **1998**, *288*, 481.

(9) Chen, J.; Rao, A. M.; Lyuksyutov, S.; Itkis, M. E.; Hamon, M. A.; Hu, H.; Cohn, R. W.; Eklund, P. C.; Colbert, D. T.; Smalley, R. E.; Haddon, R. C. *J. Phys. Chem. B* **2001**, *105*, 2525.

(10) Mawhinney, D. B.; Naumenko, V.; Kuznetsova, A.; Yates, J. T.; Liu, J.; Smalley, R. E. *Chem. Phys. Lett.* **2000**, *324*, 213.

(11) Shaffer, M. S. P.; Fan, X.; Windle, A. H. *Carbon* **1998**, *36*, 1603.

(12) Nagasawa, S.; Yudasaka, M.; Hirahara, K.; Ichihashi, T.; Iijima, S. *Chem. Phys. Lett.* **2000**, *328*, 374.

(13) Ausman, K. D.; Piner, R.; Lourie, O.; Ruoff, R. S.; Korobov, M. *J. Phys. Chem. B* **2000**, *104*, 8911.

(14) Schaefer, D. W.; Brown, J. M.; Anderson, D. P.; Zhao, J.; Chokalingam, K.; Tomlin, D.; Ilavsky, J. *J. Appl. Crystallogr.* **2003**, *36*, 553.

(15) Schaefer, D. W.; Zhao, J.; Brown, J. M.; Anderson, D. P.; Tomlin, D. W. *Chem. Phys. Lett.* **2003**, *375*, 369.

(16) Boukari, H.; Long, G. G.; Harris, M. T. *J. Colloid Interface Sci.* **2000**, *229*, 129.

(17) Morrison, J. D.; Corcoran, J. D.; Lewis, K. E. *J. Appl. Crystallogr.* **1992**, *25*, 504.
(18) Potton, J. A.; Daniell, G. J.; Rainford, B. D. *J. Appl. Crystallogr.* **1988**, *21*, 663.
(19) Jemian, P. R.; Weertman, J. R.; Long, G. G.; Spal, R. D. *Acta Metall. Mater.* **1991**, *39*, 2477.
(20) Ilavsky, J. *Particle Size ditribution from USAX, Irena SAS Modeling Macros Manual*; UNICAT: Argonne National Laboratory, Argonne, IL, USA, 2004.
(21) Monthioux, M.; Smith, B. W.; Burteaux, B.; Claye, A.; Fischer, J. E.; Luzzi, D. E. *Carbon* **2001**, *39*, 1251.
(22) Hu, H.; Bhowmik, P.; Zhao, B.; Hamon, M. A.; Itkis, M. E.; Haddon, R. C. *Chem. Phys. Lett.* **2001**, *345*, 25.
(23) Beaucage, G.; Schaefer, D. W. *J. Non-Cryst. Solids* **1994**, *172*, 797.
(24) Chen, Q.; Saltiel, C.; Manickavasagam, S.; Schadler, L. S.; Siegel, R. W.; Yang, H. *J. Colloid Interface Sci.* **2004**, *280*, 91.
(25) Schaefer, D. W.; Justice, R. S.; Koerner, H.; Vaia, R.; Zhao, C.; Yang, M.; Vale, J. *Mater. Res. Soc. Symp. Proc.* **2005**, *840*, Q3.3.1.